An implanted 4He target for experiments with radioactive beams

Weissman, L.; Raabe, R.; Huyse, M.; Koops, G.; Pattyn, H.; Terwagne, Guy; Van Duppen, P.

Published in:
Nuclear instruments and methods in physics research B

Publication date:
2000

Document Version
Publisher's PDF, also known as Version of record

ELSEVIER

Nuclear Instruments and Methods in Physics Research B 170 (2000) 266–275

NIM B
Beam Interactions with Materials & Atoms

www.elsevier.nl/locate/nimb

Letter to the Editor

An implanted ^{4}He target for experiments with radioactive beams

L. Weissman [a,*], R. Raabe [a], M. Huyse [a], G. Koops [a], H. Pattyn [a], G. Terwagne [b], P. Van Duppen [a]

[a] *Instituut voor Kern-en Stralingsfysica, University of Leuven, B-3001 Leuven, Belgium*
[b] *Laboratoire interfacultaire d'Analyses par ractions nuclaires (LARN), Facultes Universitaires N-D de la Paix, 22 Rue Muzet, B-5000 Namur, Belgium*

Received 1 November 1999; received in revised form 7 March 2000

Abstract

Solid ^{4}He targets were prepared by implantation of He ions of various energies into thin Al foils. The targets were tested using the proton Rutherford backscattering (RBS) technique. The tests showed that a considerable amount of the implanted He atoms stays in the host foils for a long time after the implantation. A possibility of using the He-implanted targets in experiments with radioactive beams is demonstrated. Further steps to increase He amount in the implanted targets are discussed.

PACS: 29.25.t; 29.25.Pj
Keywords: Implanted target; Radioactive beams

1. Introduction

Strong interest in experiments with short-lived radioactive beams is triggered by both nuclear physics and nuclear astrophysics. Of particular interest are reactions with light particles like protons, deuterons and α-particles. Since inverse kinematics is used in some of the experiments, targets made of these elements are needed. A wide variety of cryogenic, gas and solid targets is possible each with its specific merits and drawbacks. An elegant solution for reaction studies involving a radioactive ion beam has been found for hydrogen and deuterium in the form of polyethylene targets [1] and was used to measure cross-sections of proton capture reactions related to the hot CNO cycle [2,3]. Such a solution is not possible for helium and therefore a gas cell filled with helium is often used. A recent example of such an experiment with radioactive beams can be found in [4] and addresses the scattering of the halo nucleus ^{6}He on ^{4}He at relatively low beam energies (25–40 MeV).

Under certain conditions the use of a gas cell can have several disadvantages. At least four such problems were encountered in the mentioned ^{6}He–^{4}He scattering experiment [4]:

* Corresponding author. Present address: ISOLDE, CERN, CH-1211, Geneva 23, Switzerland.
E-mail address: leonid.weissman@cern.ch (L. Weissman).

0168-583X/00/$ - see front matter
PII: S0168-583X(00)00167-1

1. The 2.3 mg/cm^2 thick Al entrance and 1.8 mg/cm^2 kapton exit windows of the gas cell slow down and eventually stop particles that are scattered at specific angles.
2. The gas cell windows also scatter a non-negligible number of beam particles to the detector array. This causes a low-energy background in the Si detectors from the β-radioactivity of the beam.
3. The rather large size of the gas cell (1 cm length and 3 cm diameter) implied by the mechanical construction, does not fully match the detector geometry cutting out certain important scattering angles.
4. The large size of the gas cell also complicates the data analysis and requires an extensive Monte-Carlo simulations of the scattering events.

To avoid these difficulties we decided to prepare solid He-implanted targets for the next stage of the ^{6}He–^{4}He experiment. Using of the nobel gas implanted targets is not a novel idea. For instance, in [5], ^{3}He-implanted Nb foils were used for a measurement of the astrophysically important ^{3}He(^{4}He, γ)^{7}Be cross-section. The authors reported that with increasing ^{4}He beam fluences a significant fraction of the implanted ^{3}He (20% for a 25 mC beam fluence at a beam density below 10 μA/cm^2) escaped from the target due to heating by the impinging beam. ^{3}He-implanted targets were also produced for the ^{3}He(d, p) ^{4}He cross-section measurements [6]. As another interesting example one can mention experiments for the g-factor measurements of the first excited levels in $^{134,\,136}$Xe and in ^{40}Ar using implanted Ar and Xe targets [7,8]. Since these experiments were not dedicated to cross-section measurements, the decrease of the noble gas quantity during stable beam bombardment was not a crucial issue.

Target deterioration during the experiment is probably the limiting factor in the use of implanted targets for experiments with stable beams. However, even for most intense radioactive beam the obtained beam intensities are orders of magnitudes lower compared to stable beams. Eventually this makes the problem of target deterioration irrelevant and raises a new interest in implanted targets.

The behavior of light or noble gas ions implanted into a metal is a subject of intensive investigations. The main motivation of these studies lies in the erosion problem of walls in thermonuclear reactors due to the implantation of He and other light ions produced by nuclear reactions. Due to an extremely low He solubility, the implanted He atoms tend to cluster and to form bubbles [9]. For a relatively low He irradiation fluence of a few 10^{17} at./cm^2 the average bubble size is about 2–3 nm. A lattice of these He bubbles was observed in the metal bulk [10]. Higher implanted fluences and certain implantation profiles cause formation of large surface blisters, up to 10 μm diameter, which can burst, leaving flakes and causing wall surface erosion. This surface damage phenomenon is not completely understood. Details on the process of He-implanted bubble and blister formation can be found in [11,12] and numerous references therein.

We have chosen thin Al foils as implantation hosts, since we needed to minimize the energy losses of the scattered ^{4}He and ^{6}He particles in the host material itself. It is, moreover, well known that a large fraction of the implanted He atoms stays in the aluminum for an almost indefinite time. The formation of He bubbles and blisters in aluminum is one of the relatively well-studied cases, although the specific details of this process when implanting into thin foils are not understood. Different techniques such as Rutherford backscattering (RBS) with both regular proton beams and proton microbeams [13,14], optical absorption and electron-energy-loss spectroscopy techniques (EELS) [15], α-particle energy loss measurements [14] have been used in these studies. The most important parameter is the level of the implanted He retention, i.e., the percentage of the atoms staying in the target relative to the number of the atoms implanted, as a function of the implanted fluence, the temperature of the host during implantation, the implantation profile and the thickness of the Al host. The dependence on these different parameters complicates the understanding of the He-trapping process and leads to rather diverse results from the different experiments [13–17]. For example, during the implantation of He ions at implantation energies ranging from 0.5 to 8 keV into a 100-nm thin Al foil at room temperature, 50% He retention was observed up to an

Table 1
^{4}He fluences implanted in the three Al foils[a]

Foil	At 20 keV	At 30 keV	At 50 keV	At 80 keV	Total
#1	1.0×10^{17}	–	0	0	1.0×10^{17}
#2	0	–	0	1.0×10^{17}	1.0×10^{17}
#3	1.2×10^{17}	–	1.0×10^{17}	0.3×10^{17}	5.0×10^{17}
#4	–	4×10^{17}	–	–	–

[a] Sample #3 and #4, which was used in ^{6}He–^{4}He experiment, were implanted on both sides.

implantation fluence of 4×10^{17} at./cm^2, dropping dramatically at higher fluence [16]. In contrast, experiments with 5 keV He implanted into a 2-μm Al foil showed a maximum saturation retention of 19% and 24%, for implantation at room temperature and 120 K, respectively [14]. For implantation into a cooled target, a reemission of 40% of the retained He was observed after heating the sample to room temperature [14]. The Al film exhibited a high degree of deformation. In yet another case, a retention level of more than 90% for a similar He fluence implanted into bulk aluminum at 80 K was reported [17], though at higher fluence the retention level saturated at 40%.

More discussion of the factors which limit the implanted target thickness can be found in the early work [18] and in the more recent review paper [19].

In this work we did not try to investigate the complex physical processes involved in the He trapping in metals, but rather were pursuing the practical goal to achieve the highest possible He concentrations in the thin Al foils, and also developing a reliable method for monitoring the retained He content.

2. Experiments and results

2.1. Implantation

He-implanted Al targets were prepared at the Leuven off-line isotope separator with ^{4}He beams of various energies. The Al foil thickness was measured by weighting the samples, and was found to be 0.68 ± 0.02 μm against a nominal value of 0.8 μm, specified by the supplier, Goodfellow Cambridge Ltd. [1] The choice of the host foil thickness was dictated by the kinematics of ^{6}He–^{4}He scattering at the angles of interest and by the relatively low energy of the ^{6}He beam (29 MeV). Three probe targets were prepared. The details on the implantation doses and beam energies are listed in Table 1. The theoretical He-implantation profiles for the three targets are shown in Fig. 1. The profiles were calculated as gaussian distributions (sum of gaussians for target #3) using range and straggling parameters given by SRIM simulations [20]. SRIM simulations also showed that sputtering effects during implantation were negligible.

By using these targets we wanted to test the sensitivity of the proton RBS to as well as any dependence of the He retention level on the He implantation profile. During the implantation the He beam was scanned by applying ramp voltages on a set of vertical and horizontal plates. The beam at the target position covered a 1×1-cm^2 area. The typical pressure in the implantation chamber was kept at 10^{-8} mbar scale to avoid a build up of hydrocarbon contaminations on the target surface. The beam current was measured directly on the target itself. A positive voltage was applied to suppress secondary electrons. The beam charge was integrated, digitized and counted. During implantation the foils were mounted on an Al plate to provide heat transfer. Unfortunately, due to the small thickness and delicacy of the host foils, it was very difficult to provide a reliable thermal contact with the backing plate. In order to keep the target heating low, the He^+ current

[1] http://www.goodfellow.com/.

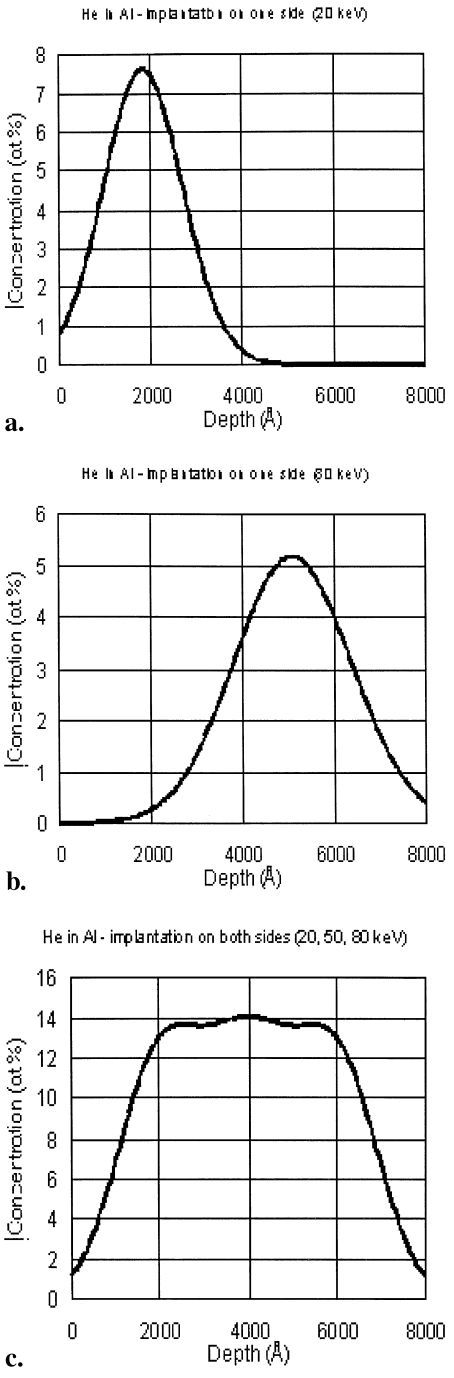

Fig. 1. Implantation profiles for ^{4}He in aluminum for three cases: (a) 20 keV beam energy; (b) 80 keV beam energy; (c) 20, 50 and 80 keV energies implanted from the both sides of the foil (Table 1).

density was kept below 4 μA/cm^2 which led to several hours of implantation time for a sample.

2.2. RBS measurements

2.2.1. Experimental procedure

To check the amount of retained He we have performed proton RBS measurements using the new Tandetron accelerator at the LARN laboratory of the University of Namur [21]. The He(p, p′)He* cross-section, σ_{He}, is much higher than the Rutherford value due to the existence of a broad and strong resonance at 2.5 MeV proton energy, corresponding to the ground state of ^{5}Li. The ratio of σ_{He} to the Rutherford cross-section at 161.4° of proton scattering angle amounts to a factor of 250 [22], allowing an accurate measurement of the retained He. The RBS measurements were carried out using a 2.2-MeV proton beam. The energy was chosen to enhance the cross-section on ^{4}He, and to have at the same time a clear separation between the ^{4}He(p, p)^{4}He peak and a small ^{27}Al(p, p′)^{27}Al* contribution. As it will be demonstrated below, the ^{27}Al(p, p)^{27}Al cross-section is equal to the corresponding Rutherford value at this particular proton energy.

The protons backscattered from the target were detected by two silicon detectors, placed at +160 and −161.4° in the laboratory frame with respect to the beam axis. The detectors distance from the target was chosen to be 100 mm. Collimators were placed in front of the detectors, giving solid angles from the center of the target of 2.6 and 1.0 msr, respectively. The proton beam current was of the order of 20 nA. The total beam intensity was measured in a Faraday cup placed behind the target. The detectors were shielded from backscattering particles originating on the Faraday cup. The proton beam dispersion due to multiple scattering within the thin Al targets was estimated to be much smaller than the entrance angle from the target to the Faraday cup aperture. One has to be careful though, in case of thicker foils or higher Z materials, to avoid errors in determination of the total beam charge due to the stronger beam dispersion in the sample. A RBS spectrum obtained

with an SnO_2-coated glass target was used for the detectors energy calibration.

The RBS measurements were carried out on the three implanted foils. A non-implanted Al sample was also tested for comparison. A typical RBS spectrum of the non-implanted sample is shown in Fig. 2(a). The small thickness of the Al foil allows to obtain a high quality RBS spectrum. Beyond a strong RBS Al peak, two resolved peaks of ^{16}O and two resolved peaks of ^{12}C corresponding to the aluminum oxide and carbon layers at the front and the rear foil surfaces are clearly visible. A weak peak around 900 keV corresponding to a non-elastic $^{27}Al(p, p')^{27}Al^*$ scattering is also observed. The RBS spectrum of the non-implanted target exhibits a low background in the lower-energy region. This provides a possibility for a reliable measurement of the He-implanted samples. The RBS spectrum of target #3 with the largest implanted amount is shown in Fig. 2(b), where a strong He RBS peak is clearly observed. The comparison of the RBS He peaks for targets #3, #1, #2 and #1, reversed with respect to the proton beam direction, is shown in Fig. 3 (see the theoretical implantation profiles in Fig. 1). The sensitivity of the RBS peak to the implantation profile is clearly demonstrated. One can also observe that the high-energy side of the RBS peak is much steeper than the low-energy one, due to straggling of protons backscattered from the deeper implanted He atoms. The narrowest RBS peak of non-reversed target #1 corresponds to the most shallow implantation profile.

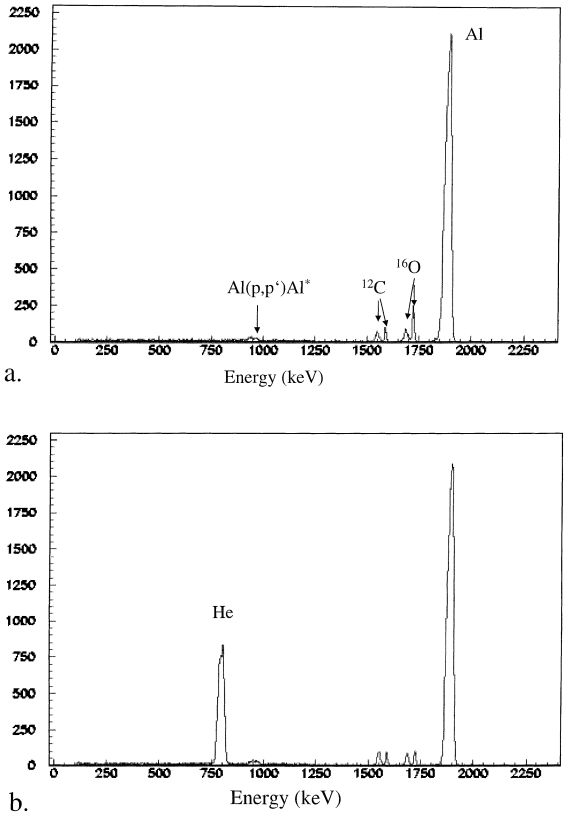

Fig. 2. The RBS spectra of (a) the non-implanted Al sample, (b) target #3. The peak from the He signal is clearly visible. One can also observe the fine structures of the RBS spectrum: the resolved ^{16}O and ^{12}C peaks from the two foil surfaces and a weak peak from non-elastic $Al(p, p')Al^*$ scattering.

2.2.2. Results

The content of the implanted He, N_{He}, was determined from the ratios of the integrals of the He, Y_{He} and Al, Y_{Al}, RBS peaks and the known number of Al atoms in the foil, N_{Al},

$$N_{He} = \frac{Y_{He}}{Y_{Al}} \frac{\sigma_{Al}}{\sigma_{He}} N_{Al}, \quad (1)$$

with σ_{He} and σ_{Al} being the $^4He(p, p)^4He$ and $^{27}Al(p,p)^{27}Al$ cross-sections values.

The $^{27}Al(p, p)^{27}Al$ cross-section oscillates substantially around the Rutherford values [22].

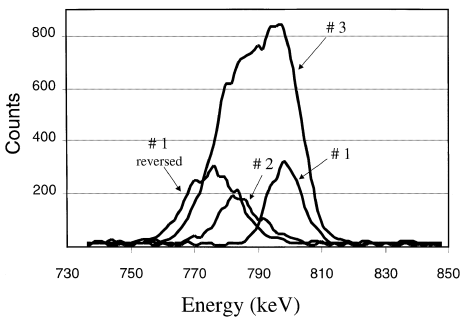

Fig. 3. The comparison for the RBS He peak for #3, #1, #2 and reversed #1 foils (see the theoretical implantation profiles in Fig. 1). The RBS sensitivity to the implantation profile is clearly demonstrated.

However, it is known that the cross-section is equal to the Rutherford value at 2.2 MeV proton energy. To check this we have performed an energy scan around 2.2 MeV, comparing the cross-section obtained from the Al RBS yield per proton beam charge measured in the Faraday cup and the calculated Rutherford value. The results of this comparison are shown in Fig. 4. The main error of the calculated cross-section comes from the uncertainties of the foil thickness (3%). The measurement demonstrates that indeed around 2.2 MeV the ^{27}Al(p, p)^{27}Al cross-section is equal to the Rutherford one (51.40 mb).

The retained He quantities are shown in Table 2. The values show that the targets are characterized by a high He retention level of 30–50%.

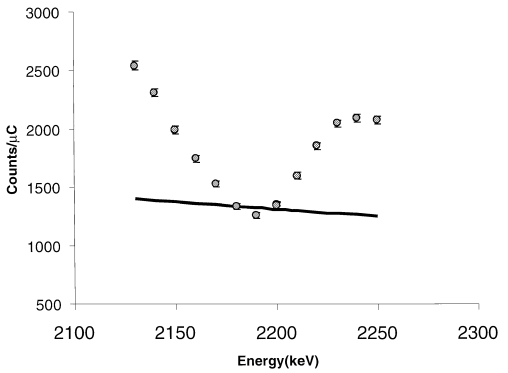

Fig. 4. Yields of ^{27}Al(p, p)^{27}Al backscattering events at energies around 2.2 MeV, for a proton beam dose of 2.0 μC. The solid line is the calculated Rutherford yield for a Al foil thickness of 0.68 μm. The estimated error on the calculated Rutherford cross-section is 3%.

Table 2
Results of the RBS measurements: detected ^{4}He thickness in the different foils

Foil	^{4}He content (cm^{-2})	^{4}He at.%	Retention (%)
#1	$(4.98 \pm 0.18) \times 10^{16}$	1.2	50
#2	$(3.02 \pm 0.14) \times 10^{16}$	0.7	30
#3	$(2.20 \pm 0.07) \times 10^{17}$	5.4	44
#4	$(2.72 \pm 0.04) \times 10^{17}$	6.6	34

3. Discussion

The high retention level in all targets seems to indicate that the long time elapsed between the implantation and the RBS measurements (three weeks) did not cause significant diffusion of ^{4}He from the host foil, even though no particular procedure was followed to store the foils. The retention level in target #2 is significantly smaller, which might be due to higher energy deposition in the target during the implantation at 80 keV. However, since the surface of target #2 was slightly damaged, which also can cause a lower He RBS yield, it is not possible to draw firm conclusions concerning the He retention dependence on the implantation energy.

It is interesting to compare scanning electron microscope (SEM) images of the Al foil prior to (Fig. 5(a)) and after implantation (Fig. 5(b)). While the untreated foil demonstrates a crystalline structure, the implanted sample (target #3) has a completely smooth surface. No He bubbles were observed in the SEM images. The SEM image of the surface next to the implanted area does not differ significantly. Therefore the foil structure modification is probably due to the heating by the beam during implantation.

The θ–2θ X-ray diffraction measurements of the non-implanted sample and target #3 were performed in the Bragg–Brentano configuration at 1.541 Å (CuK_α). The X-ray diffraction spectra (Fig. 5(c) and (d)) indicate that the modification in the crystalline structure due to the beam impact is not only limited to the surface but also extends into the bulk material. From the FWHM of the diffraction peaks an average grain size of 60 and 35 nm can be deduced for the untreated and #3 targets, respectively. The drastic modification of the foil crystalline structure during the implantation is an interesting phenomenon. It is not clear at present how it affects the He trapping process.

The obtained retention levels are similar for targets #3 and #2, while the atomic concentration of ^{4}He varies by a factor 5. It is therefore possible that the saturation concentration of ^{4}He in target #3 was not reached. Although the He content of the target #3 is sufficient for our experiment, we have tried to achieve a higher amount in further

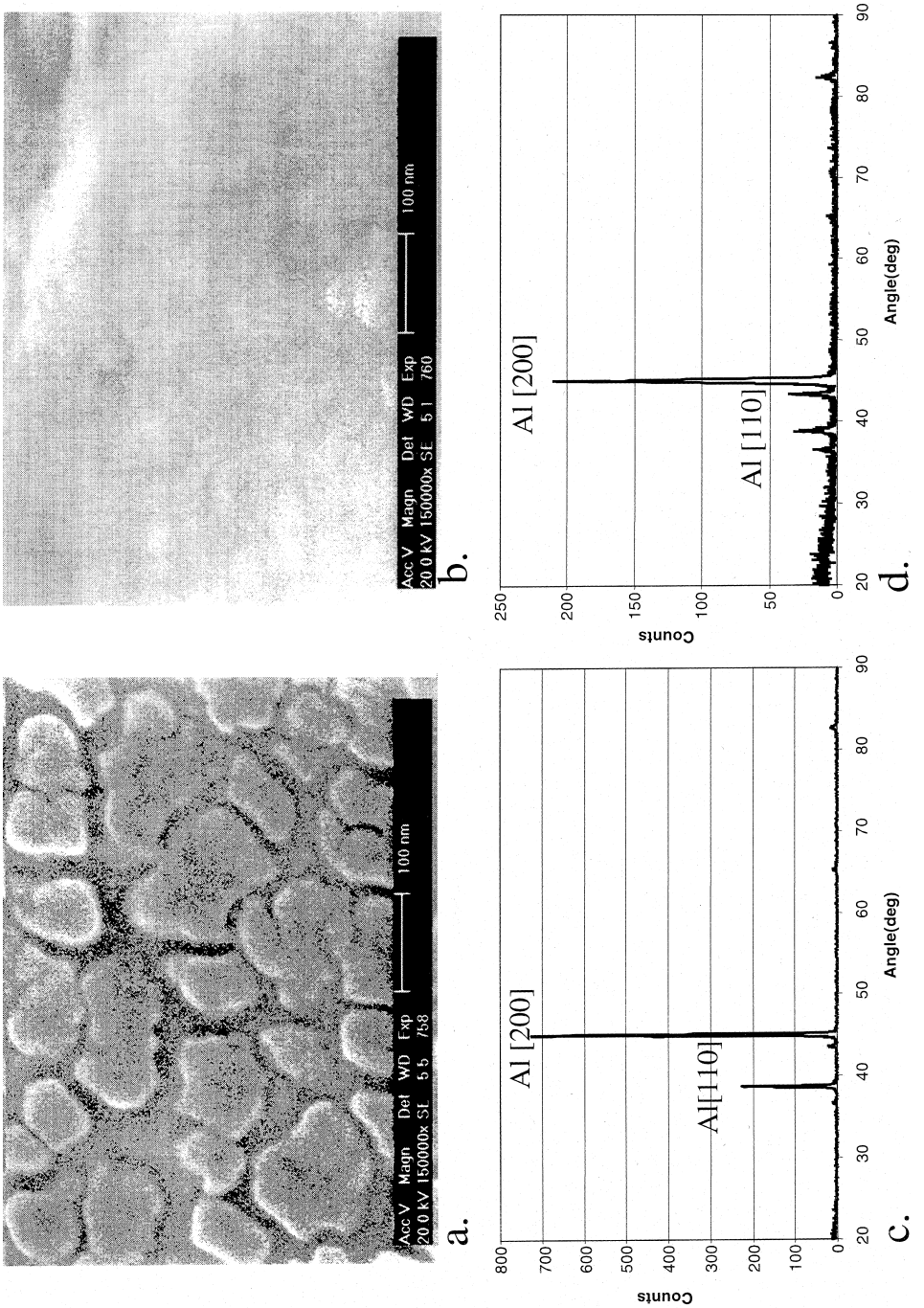

Fig. 5. (a) and (b) The SEM images of untreated Al foil and the #3 target. (c) and (d) The corresponding X-ray spectra. The diffraction peaks corresponding to the [1 1 0] and [2 0 0] Al lattice planes are indicated for both cases.

implantations. We have performed a few additional implantations with the beam fluences higher than 10^{18} at./cm^2. The RBS measurements of these samples showed retention levels below 30%. It is not clear whether the poor retention is due to target heating during the implantation or due to a massive re-emission of He above some critical concentration value as seen in [14,16,17]. The target surfaces reveal severe deformations, though it does not appear to be the result of He blisters. For a sample with an especially deformed surface several RBS measurements were performed for different beam spot positions on the target surface. The ratio of He and Al RBS peak integrals was found to be constant within 5%.

For the final target (#4 target), used in the ^{6}He experiment, we aimed at a compromise with fluences of 4×10^{17} He ions implanted into both sides of the foil. By implanting into two sides of the foil we have reduced the local He concentration avoiding critical He density limits. An implantation energy of 30 keV was chosen to reduce the target heating and at the same time to have a reasonably deep profile. The amount of the final target was $(2.72 \pm 0.04) \times 10^{17}$ at./cm^2 which correspond to a 34% retention level and 6.6% atomic concentration of the trapped He (Tables 1 and 2). For comparison the effective thickness of the gas cell target used in the previous experiments [4] was 1.2×10^{19} at./cm^2. With the procedures presently in use, it seems that the maximum concentration of the He atoms in the 0.7 μm thickness Al foils is limited to 7%. As this is probably due to heating during the implantation process, a better heat transfer should be envisaged. As the only feasible solution of this problem one can suggest a procedure such as described in [23], where the thin implantation host was evaporated on a thick copper substrate, which was removed after implantation by dissolving in 7 N HNO_3 solution.

Target #4 has been used in the second stage of the ^{6}He–^{4}He experiment [4]. The increase of the ^{6}He beam intensity at the Louvain-la-Neuve facility compared to the previous experiment [4] was very important for the success of this experiment and the analysis is in progress. It is interesting to compare some selected numbers from the two experiments in order to see the differences between the gas and implanted targets (Table 3). In Fig. 6(a) and (b), the correlation spectra obtained by detecting simultaneously two particles in two sectors of the LAMP array [4,24] are given. A few interesting features emerge from the comparison of the numbers in Table 3 and spectra from Fig. 6(a) and (b).

1. In both spectra, the events corresponding to ^{6}He–^{4}He elastic scattering are clearly visible, but in the gas cell these events are not lying on a straight-line but rather on a "bow-like" structure due to the difference in the particle energy loss in the gas cell windows as a function of the angle under which the particle leaves the gas cell.
2. There is an additional strong background in the gas cell spectrum due to p(^{6}He, ^{4}He)^{3}H reaction with hydrogen nuclei from the gas cell exit window (Fig. 6(a)).
3. As seen from Table 3, the background rate in the case of the implanted target is much lower than for the gas target. However, the ratio of the rates of the detected ^{6}He–^{4}He scattering events to the background events is better for the gas target. To improve this figure or merit a larger content of He in the implanted target has to be obtained.
4. As in case of the implanted target, all scattering events are originating from a well-localized geo-

Table 3
Comparison of the experiments with the gas cell [4] and the implanted target[a]

	# of ^{4}He (10^{17})	^{6}He dose (nC)	# $M = 2$ events	# ^{4}He–^{6}He	Background rate (pC^{-1})	^{4}He–^{6}He rate (pC^{-1})
Gas cell	1200	0.29	64144	1834	221.2	6.3
Implanted	2.7	4.9	52139	652	10.6	0.13

[a] Multiplicity $M = 2$ events are presented for LAMP–LAMP coincidences only. An energy threshold of 2 MeV was used. The ^{4}He–^{6}He coincidences detected in the $70° \leqslant \theta_{c.m.} \leqslant 125°$ range are presented.

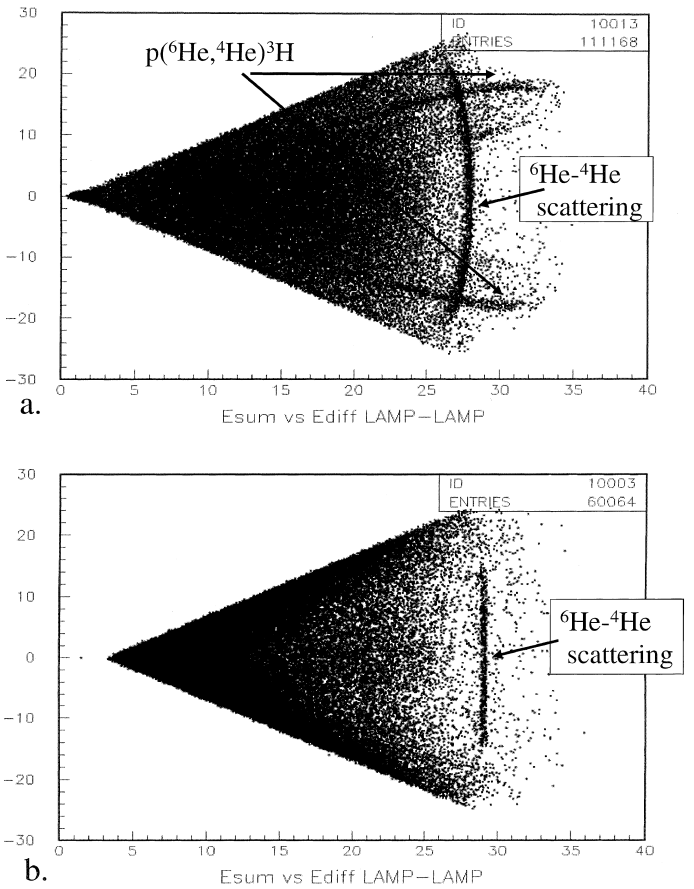

Fig. 6. ^{6}He–^{4}He correlation spectra of the energy sum versus energy difference of the two particles simultaneously detected in the LAMP array for the gas cell target (a) the implanted target (b).

metrical position, the analysis of the data is straightforward.

About two months after the experiment, the He content of the used target was remeasured with the proton RBS. The He content in the target was found to be the same.

4. Conclusion

We have demonstrated that solid He-implanted targets can be used in experiments with radioactive beams. By utilizing the implanted He target we could overcome several difficulties of the previous ^{6}He–^{4}He scattering experiment where a gas cell was used. This work can serve as a benchmark for further use of He-implanted targets for experiments with radioactive beams. The improvement of the implantation procedure by arranging a reliable heat transfer may allow to further increase the implanted amount. However, we want to point out that previous implantation studies, which were performed as function of implantation energy, host thickness and implantation temperature [14,16,17], showed that an implanted fluence of $4–7 \times 10^{17}$ at./cm^2 seems to be the limit above which the He atomic concentration either reaches saturation (5–7% for 0.7 μm Al film) or drops due to the massive He reemission. For instance, the high ^{3}He fluences in [6] (more than 10^{19} ions/cm^2) has resulted to a relatively small ^{3}He content ($1–2 \times 10^{17}$cm^{-2}).

For those experiments, where the host foil thickness is not an issue, higher implanted He amount could be obtained eventually by applying the technique of simultaneous implantation of He and evaporation of the host material [8] or He implantation into a carbon layer, built up during the implantation on the target surface [25].

As an interesting possibility one can consider the preparation of He implanted targets using the relatively novel plasma immersion implantation technique, where large implantation fluences can be implemented in a short time [26].

Acknowledgements

We express our gratitude to Mr. Y. Morciaux for operation of the LARN accelerator and Mr. W. Schollaert for his help in operating the Leuven off-line separator. We want to thank Dr. R. De Vos and Dr. Kr. Temst for their assistance in the SEM and the X-ray measurements. We also would like to acknowledge the excellent performance of the Louvain-la-Neuve accelerator crew during the ^{6}He–^{4}He experiment.

References

[1] W. Galster et al., Phys. Rev. C 44 (1991) 2776.
[2] P. Decrock et al., Phys. Rev. Lett. 67 (1991) 808.
[3] C. Michotte et al., Phys. Lett. B 381 (1999) 402.
[4] R. Raabe et al., Phys. Lett. B 458 (1999) 1.
[5] T.K. Alexander, G.C. Ball, W.N. Lennard, H. Geissel, Nucl. Phys. A 427 (1984) 526.
[6] W.H. Geist, Z. Ayer, A.C. Hird, E.J. Ludwig, M. Wood, K.A. Fletcher, Nucl. Instr. and Meth. B 111 (1996) 176.
[7] K.H. Speidel, H. Busch, S. Kremeyer, U. Knopp, J. Cub, M. Bussas, W. Karle, K. Freitag, U. Crabowy, J. Gerber, Nucl. Phys. A 552 (1993) 140.
[8] U. Grabowy, H. Bush, A. Gohla, K.-H. Speidel, S. Kremeyer, G. Jakob, K. Freitag, J. Gerber, W. Assman, Nucl. Instr. and Meth. B 101 (1995) 422.
[9] H. Ullmaier, Radiat. Eff. 78 (1983) 1.
[10] P.B. Johnson, in: S.E. Donnelly, J.H. Evans (Eds.), Fundamental Aspects of Inert Gases in Solids, NATO ASI series B 279 (1991) 167.
[11] E.P. EerNisse, S.T. Picraux, J. App. Phys. 48 (1977) 9.
[12] J.H. Evans, J. Nucl. Mater. 68 (1977) 129.
[13] F. Bodart, S.E. Donnelly, Nucl. Instr. and Meth. 218 (1983) 529.
[14] S.E. Donnelly, F. Bodart, K.M. Barfoot, R. Wernz, R.P. Webb, Thin Solid Films 94 (1982) 289.
[15] J.C. Rife, S.E. Donnelly, A.A. Lucas, J.M. Gilles, J.J. Ritsko, Phys. Rev. Lett. 46 (1981) 1220.
[16] W. Jäger, R. Manzke, H. Trinkaus, G. Crecelius, R. Zeller, J. Fink, H.L. Bay, J. Nucl. Mater. 111–112 (1982) 674.
[17] K.L. Wilson, G.J. Thomas, J. Nucl. Mater. 63 (1976) 266.
[18] O. Almen, G. Bruce, Nucl. Instr. and Meth. 11 (1961) 257.
[19] B.M. Scherzer, in: R. Behrish (Ed.), Sputtering by Particle Bombardment II, Springer, Heidelberg, 1983, p. 271.
[20] J.F. Ziegler, Stopping Powers and Rangers in All Elements, Vol. 4, Pergamon, New York, 1977; SRIM 1998 version.
[21] G. Demortier, Nucl. Instr. and Meth. B 66 (1992) 51.
[22] J.R. Tesmer, M. Nastasi, Handbook of Modern Ion Beam Material Analysis, Materials Research Society, Pittsburgh, USA, 1995.
[23] G. Terwagne, S. Lucas, F. Bodart, G. Sorensen, H. Jensen, Nucl. Instr. and Meth. B 45 (1990) 95.
[24] P.J. Sellin, Nucl. Instr. and Meth. 311 (1992) 217.
[25] A. Arnesen, T. Noreland, L.O. Norlin, Phys. Scr. 11 (1975) 351.
[26] J. Min, P.K. Chu, X. Lu, S.S. Kumar Iyer, N.W. Cheung, Thin Solid Films 300 (1997) 64.